European Polymer Journal 98 (2018) 116–124

Contents lists available at ScienceDirect

European Polymer Journal

journal homepage: www.elsevier.com/locate/europolj

Physical and mechanical properties of a vegetable oil based nanocomposite

Juan M. Buffa[a], Gurutz Mondragon[b], M. Angeles Corcuera[b], Arantxa Eceiza[b], Verónica Mucci[a,*], Mirta I. Aranguren[a]

[a] Instituto de Investigaciones en Ciencia y Tecnología de Materiales (INTEMA), Universidad Nacional de Mar del Plata-CONICET, Juan B Justo 4302, 7600 Mar del Plata, Argentina

[b] Materials + Technologies Group (GMT), Department of Chemical and Environmental Engineering, Polytechnic School, University of the Basque Country (UPV/EHU), Plaza Europa 1, 20018 Donostia-San Sebastián, Spain

ARTICLE INFO

Keywords:
Vegetable oil
Cellulose nanocrystals
Nanocomposite
Mechanical properties

ABSTRACT

Nanocomposites films were prepared from a bio-based waterborne polyurethane and cellulose nanocrystals (CNCs) obtained from the sulfuric acid hydrolysis of cellulose nanofibers. The polyurethane used as matrix of the nanocomposite film was synthesized from a biobased macrodiol derived from castor oil, 2,2-bis(hydroxymethyl) propionic acid, 1,6-hexamethylene diisocyanate and triethylamine. The concentration of CNC in the films was varied from 0 to 10 wt.%, and the films obtained by casting were characterized by DSC, DMA, tensile tests and TGA. Due to the hydrophilic nature of the PU, the nanocrystals were well dispersed, obtaining homogenous and transparent films which displayed improved thermal and mechanical properties compared to the neat PU. The impact of the CNCs on the crystallization of the polymer was analyzed. Finally, the mechanical properties were fitted to well known theoretical models, allowing a better understanding of the interactions between polymer and filler in the composites.

1. Introduction

Over the last decades, the interest on developing environmentally friendly materials has grown exponentially, as the consciousness for a sustainable development has become more and more widespread [1–5]. In particular, there is also an increasing interest in the replacement of synthetic reinforcements in composites by natural fibers/particles, due to their renewability and low environmental impact [4,6].

One of the main objectives is the replacement of non-renewable resources for renewable ones, such as the cellulose, which is a structural component of the cell wall of plants [7–9]. Usually, cellulose is processed in different ways to obtain technically better materials, particularly, cellulose nanocrystals (CNCs). They are rod-like particles with width in the range of 2–20 nm and lengths that can reach several hundreds of nanometers, and can be isolated from microfibrillated or microcrystalline cellulose among other numerous sources using mechanical or chemical (enzymatic or acid hydrolysis) methods or a mixture of both [8]. CNCs are ideal candidates as nanotechnologic materials because of their rod-like nanostructure, abundance, biodegradability, renewability and multi-functionality, with the result that for some applications they can replace high-cost, non-biodegradable synthetic fibres, for example, carbon nanotubes [10].

The most important properties of CNC are its mechanical properties, such as very high modulus, theoretically 124–172 GPa, while experimentally 12–150 GPa with a high dispersity of results [11–16], a very low density, resulting in a specific tensile modulus (tensile modulus/density) higher than steel's (85 vs 25 kJ kg^{-1}) [17]. Because of this, CNC are very good candidates as reinforcement for polymeric nanocomposites. Nevertheless, cellulose is a carbohydrate, and as such, it has many hydroxyl groups in the surface, making it more attractive in combination with polar matrices. Also, when using non-polar polymers, the CNC can be superficially modified, however it must be considered that surface modification also reduces the interaction among the CNC, reducing the reinforcing effect, thus a balance between dispersion and cellulose interaction must be found in such cases [18].

On the other hand, polyurethanes (PUs) are a family of polymers that has been used for several applications in a wide range of products such as biomedical, coatings, foams, adhesives and composites [19]. In particular, segmented PUs are copolymers with a structure of alternated soft and hard segments, the first ones consisting mainly of the long chains of polyol/macrodiol, and the latter being formed by the isocyanate and the chain extender usually added to these formulations. The large variety of available polyols and isocyanates leads to the high versatility of the PUs [20,21]. Conventional PUs are synthesized using organic solvents, but with the increasing interest in using eco-friendly materials, the development of waterborne polyurethanes (WBPUs) has

* Corresponding author.
E-mail address: vmucci@fi.mdp.edu.ar (V. Mucci).

https://doi.org/10.1016/j.eurpolymj.2017.10.035
Received 12 June 2017; Received in revised form 27 October 2017; Accepted 31 October 2017

been promoted [22,23]. In this case, the use of WBPUs as polymer matrix, restricts the available fillers to those with hydrophilic nature, and once again, CNCs are ideal candidates [24].

In this study, a WBPU was synthesized using a natural macrodiol derived from castor oil and 1,6-hexamethylene diisocyanate (HDI) and it was used as the matrix for cellulose nanocomposites. The CNCs used in this study were prepared from cellulose nanofibers derived from Kraft pulp by acid hydrolysis. The composites obtained were characterized by their thermal and mechanical properties.

2. Materials and methods

2.1. Materials

Microfibrillated cellulose (MFC) was provided by University of Maine and was hydrolyzed using sulfuric acid (96%, Aldrich) [25]. For the synthesis of the WBPU, 2,2-bis(hidroxymethyl)propionic acid (DMPA, 96%, Aldrich), 1,6-hexamethylene diisocyanate (HDI, 98%, Aldrich), triethylamine (TEA, 99%, Aldrich), dibutyltin dilaurate (DBTDL, 95%, Aldrich) and acetone (technical grade, Aldrich) were used. The macrodiol used was derived from castor oil, with the chemical structure showed in Fig. 1 and M_n of 1320 g mol^{-1} [21,26].

2.2. Methods

2.2.1. Acid hydrolysis

To obtain the CNCs, an acid hydrolysis was performed. 103.9 g of MFC with a solid content of 3.85 wt.% (4 g of dried MFC) where mixed with 414.3 g of distillated water, cooled in an ice bath and strongly stirred. Once the temperature was stable around 2 °C, 514.5 g of H_2SO_4 96% were slowly added (1 h). Then the temperature was risen to 44 °C and kept at that value for 1 h. To finish the reaction, the mixture was diluted to a final volume of 1 L. Then, it was dialyzed against distilled water for one week until reaching a pH around 5 and stored at 4 °C [9,27,28]. Once the suspension was obtained, the solid content was determined by drying a small amount of the suspension at 50 °C overnight, and weighing the dried solids. The procedure was performed by quadruplicate.

2.2.2. Synthesis of WBPU

For the synthesis of the WBPU, a one-step procedure was used [21,29]. The macrodiol was dried in rotary evaporator for one day prior to use, then 18 g were weighed and taken to 80 °C under strong stirring. Then 1.15 g of DMPA (acting as internal emulsifier), 4 drops of DBTDL (catalyst) and 4.47 g of HDI were added in that order (slow addition in the case of HDI). The reaction was performed for 4 h, but during the last 2 h the temperature was reduced to 60 °C and 100 mL of acetone were added in aliquots of 10 mL, to diminish the viscosity of the reaction medium. Finally, to neutralize the ionic groups, TEA was added and heating was turned off. When the system reached room temperature, 100 mL of water were added and the system was gently stirred overnight. Rotary evaporation was used to eliminate any trace of acetone from the suspension.

2.2.3. Preparation CNC/WBPU films

The nanocomposites were prepared adding different percentages of CNC (0, 1, 3, 5 and 10 wt.%, dry basis) to the polymer. The needed amount of the CNCs suspension (originally 1.108 wt.%) was mixed with water (when required) and stirred overnight, as well as the WBPU suspension. The addition of water to the cellulose suspension was performed to keep the total liquid weight equal for all the nanocomposites prepared and thus reducing differences in drying times. The CNCs suspension was sonicated during 30 min and then mixed with the already prepared (fully reacted) WBPU dispersion, stirred for 5 min and sonicated for 30 min more. The films were obtained by solvent casting in a Petri dish with PTFE/Teflon coating for 24 h at 50 °C [30].

2.2.4. Characterization

Atomic force microscopy was performed using an AFM Multimode Bruker, using tapping mode at a scan rate of 0.996 Hz, 512 samples per line, amplitude set point between 350 and 400 mV and drive amplitude between 100 and 150 mV.

The crystalline index (CI) of the CNCs was evaluated by X-ray diffraction, using a PHILIPS X'PERT PRO automatic diffractometer equipped with a Cu(Kα) radiation source (λ = 0.1546 nm). Data was collected from 2θ = 5 to 80° at a scanning rate of 0.026°/s. Crystalline peaks 1–10, 110, 102, 200 and 004 appear at 2θ: 14.6°, 16.8°, 20.2°, 22.7° and 34.7°, respectively [31–33]. The CI was calculated, after performing the deconvolution of the crystalline peaks and the amorphous contribution, as the ratio of the area under the crystalline peaks to the total area in the range 10–36° [34].

Dynamic light scattering (DLS) was used to measure the size of WBPU particles in the dispersion. Using a Malvern Zetasizer Nano S-90 with a laser of 632 nm (Malvern Instruments Co. Ltd., Worcestershire, UK), at 25 °C on the samples highly diluted in deionized water.

The color of the films was determined using a LOVIBOND Reflectance Tintometer RT Series. The data obtained from the equipment is expressed as L, a and b (lightness, red-green and yellow-blue indexes, respectively). The total color difference (ΔE) and whiteness index were calculated by Eqs. (1) and (2) respectively, considering the neat WBPU as Ref. [35].

$$\Delta E = \sqrt{(\Delta L)^2 + (\Delta a)^2 + (\Delta b)^2} \quad (1)$$

$$WI = 100 - \sqrt{(100 - L)^2 + a^2 + b^2} \quad (2)$$

WBPU, CNC and nanocomposites characteristic functional groups were analyzed by Fourier transform infrared spectroscopy (FTIR) using a Nexus Nicolet spectrophotometer, by attenuated total reflection (ATR) technique with a ZnSe crystal. 64 scans with a resolution of 8 cm^{-1} were averaged to obtain each spectrum. The spectra were normalized using the peak at 2930 cm^{-1} for easier comparison.

A Jeol JSM-6460LV scanning electron microscope operating at 15 kV was used to observe the fragile fracture surface of the composites obtained under liquid nitrogen. Previously, the samples were sputter-coated with a thin layer of a mixture of gold and palladium.

Differential scanning calorimetry (DSC) thermograms were obtained using a DSC Mettler Toledo 822 under N_2 atmosphere, and performing scans in three steps: from −75 °C to 200 °C at 20 °C min^{-1}, then to −75 °C at −5°C min^{-1} and finally to 180 °C at 20 °C min^{-1}. The glass transition temperature was determined as the midpoint of the heat capacity change. ΔH is calculated based on the weight of the polymer in the composite.

Dynamic mechanical analysis (DMA) was performed using a Gabo Eplexor 100 N, performing temperature scans from −100 °C to 100 °C

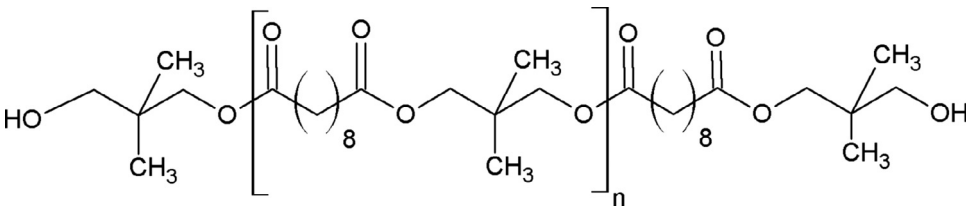

Fig. 1. Chemical structure of the macrodiol used.

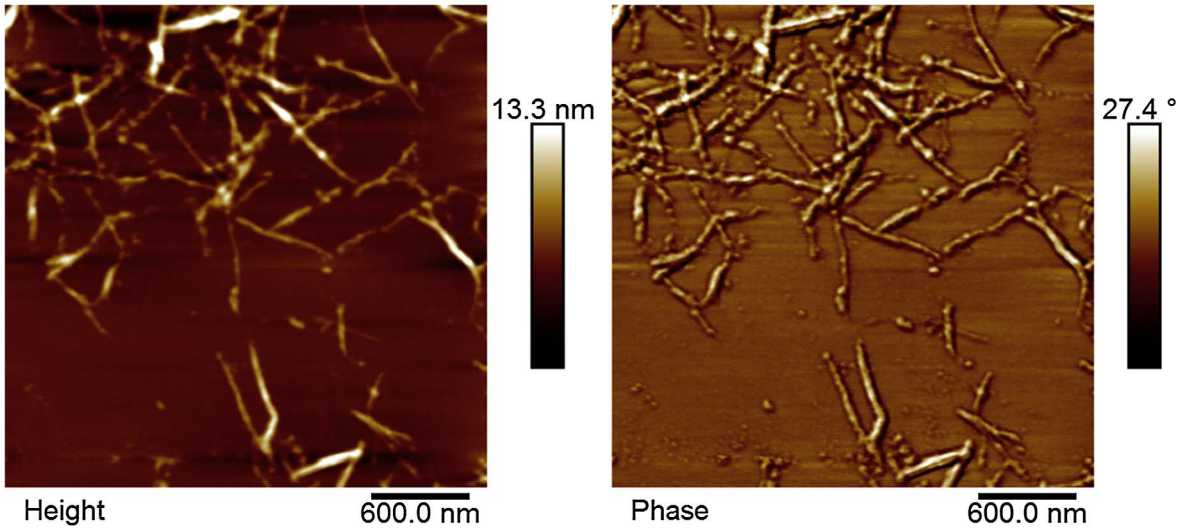

Fig. 2. AFM micrographs of CNC.

at a scanning rate of 2 °C min^{-1} at a frequency of 10 Hz, using probes of 3 mm in width, 50 mm in length and specimen thickness in the range of 0.3–0.6 mm, measured for each sample with a caliper (± 0.001 mm).

Tensile tests were performed using a MTS Insight 10 with a load cell of 250 N. The samples were cut in strips of approximately 3 mm in width, 50 mm in length and thickness in the range of 0.3–0.6 mm, measured for each sample with a caliper (± 0.001 mm). The pneumatic grips were separated 8 mm and the test was performed at a speed of 10 mm min^{-1}.

The values of the modulus of the composites were fitted using two different models: Hirsch and Ouali. The first one uses the well-known parallel and series models, that consider uniform strain and uniform stress in the composite, respectively, resulting in Eqs. (3) and (4),

$$E_c = E_m\varphi_m + E_f\varphi_f \tag{3}$$

$$E_c = \frac{E_m E_f}{E_m\varphi_f + E_f\varphi_m} \tag{4}$$

where E_m and E_f are the modulus of the matrix and the filler respectively, and φ_m and φ_f the respective volume fractions. Eq. (3) corresponds to the upper bound and Eq. (4) to the lower one [36]. However, the actual modulus falls between these limits, and the Hirsch model considers this complex behavior by simply combining the previous predictions according to Eq. (3)

$$E_c = x(E_m\varphi_m + E_f\varphi_f) + (1-x)\frac{E_m E_f}{E_m\varphi_f + E_f\varphi_m} \tag{5}$$

where x and (1 − x) are the fractional contributions of the parallel and series models to the actual modulus of the composite [37]. However, this simple model cannot reproduce the presence of a percolation threshold that may appear in nanocomposites. For this reason, Ouali model was also used to represent the experimental data. In this case Eq. (6) is used.

$$E_C = \frac{(1-2\psi + \psi\varphi_f)E_m E_f + (1-\varphi_f)\psi E_f^2}{(1-\varphi_f)E_f + (\varphi_f-\psi)E_m} \tag{6}$$

with φ_f being the volumetric fraction of filler, while ψ is calculated from Eqs. (7) and (8)

$$\psi = 0 \qquad \varphi_f < \varphi_c \tag{7}$$

$$\psi = \varphi_f\left(\frac{\varphi_f-\varphi_c}{1-\varphi_c}\right)^{0.4} \qquad \varphi_f > \varphi_c \tag{8}$$

where φ_c is the concentration of the filler at which percolation is reached and can be estimated using Eq. (9)

$$\varphi_c = 0.7\left(\frac{d}{L}\right) \tag{9}$$

where L is the length and d the diameter of the filler [3].

In the case of the strength of the composites, the model proposed by Pukanzsky et al. has been used [38,39]. It considers that the dependence of the stress at yield with the content of filler is determined by the decrease of the effective load bearing cross section of the matrix due to filling and by the polymer-filler interaction. Both effects are considered in Eq. (10)

$$\sigma_y = \sigma_{y0}\left(\frac{1+\varphi_f}{1+2.5\varphi_f}\right)e^{B\varphi_f} \tag{10}$$

where σ_y is the stress at yield of the composite, σ_{y0} corresponds to that of the neat WBPU, φ_f is the volume fraction of CNCs and B is a parameter that characterizes the interfacial interaction. Use of this equation by different authors has demonstrated that when B is higher than 3, there is good interfacial adhesion and a reinforcing effect is obtained [37,40]. The volumetric fractions were calculated from the experimental weight fractions and using density values of 1.08 and 1.50 g/cm^3 for the polymer and CNC, respectively [23,41].

The thermogravimetric analysis was performed using a TGA/SDTA 851 Mettler Toledo, under N_2 atmosphere, from room temperature to 800 °C at 10 °C min^{-1}.

3. Results and discussion

3.1. CNC characterization

The CNCs obtained were characterized by AFM (Fig. 2) and measured in thickness and length using the height images, analyzing a population of over 50 CNCs. The AFM images are representative of the topography and phase of the nanocrystals; the diameter determined is 5.6 ± 1.4 nm and the length 294.5 ± 81.3 nm, dimensions that are in agreement with usually reported data [5,8,42,43]. The CI calculated from DRX is 61.9%, which is within the usually reported interval [32].

3.2. WBPU characterization

DLS was used to measure the size of the particles of the WBPU synthesized, obtaining a size of particles of 33.21 ± 6 nm, which is acceptable since it has been reported that particle sizes between 20 and 200 nm produce stable dispersions and form homogeneous films [29].

Table 1
Colorimetric data of the neat WBPU and composites films.

CNC (wt.%)	L	a	b	ΔE	WI
0	86.57 ± 0.57	0.67 ± 0.04	−3.80 ± 0.23	–	86.03 ± 0.21
1	85.05 ± 0.71	1.22 ± 0.24	−2.01 ± 0.83	2.28	85.05 ± 0.63
3	86.38 ± 0.21	0.80 ± 0.07	−2.58 ± 0.28	1.24	86.11 ± 0.20
5	87.08 ± 0.28	0.77 ± 0.06	−2.86 ± 0.13	1.07	86.85 ± 0.12
10	87.61 ± 0.50	0.77 ± 0.03	−3.02 ± 0.44	1.30	87.22 ± 0.39

3.3. Nanocomposites characterization

3.3.1. Colorimetric characterization

Table 1 summarizes the values from the colorimetric characterization of the films. As can be seen, the L index is similar for all the samples and in all cases higher than 85%, indicating that all the films are transparent, and that there was a very good dispersion of the CNC, even in the films with high concentrations of the nanofiller. Regarding redness (a) and yellowness (b) there is not a clear trend, however all the composites are more yellow and red than the neat WBPU, particularly the one with 1 wt.% of CNC. The whiteness (WI) remain approximately constant and follows closely the lightness index, while the total color difference (ΔE) is negligible [35]. In general, from this data it can be concluded that the appearance of the films is essentially not modified by the presence of CNC, probably because of its nano-size and its good dispersion in the composites.

3.3.2. FTIR

Fig. 3 shows the FTIR spectra of the samples. The CNCs show the expected spectrum, with the strong band between 3000 and 3400 cm^{-1} due to the OH stretching, the band at 2900 cm^{-1} due to stretching of CH and several peaks between 1430 and 1000 cm^{-1} assigned to different deformations of cellulose rings, such as the C−C ring stretching band (1160 cm^{-1}), C−O−C glycosidic ether group band (1106 cm^{-1}), pyranose ring stretching vibration bands (1053 and 1027 cm^{-1} [4,44,45]. The spectra of the composites show the expected peaks of the polyurethane, such as the amide-I (ester C═O and urethane C═O) at 1730 cm^{-1}, the amide-II (N−H bending and N═C═O asymmetric stretching) at 1520 cm^{-1} and the NH stretching vibration at 3300–3400 cm^{-1}. As the amount of CNC in the composites increases from 0 to 10 wt.%, the absorbances at 3350 and 1035 cm^{-1} increase, as those are the zones where the cellulose presents high absorbance, as already mentioned. There is a small decrease in the absorbance of the peak at 1520 cm^{-1}, because the amount of WBPU in the composite diminishes (in percentage) with the addition of CNCs [27,46,47], and the CH peak at 2900 cm^{-1} (present in polymer and CNC) was chosen to normalize the spectra.

3.3.3. SEM fracture micrographs

The fragile fracture micrographs are shown in Fig. 4. A very clear and important change is observed when CNC is added, even at the lowest concentration used in this study. The increase in roughness is the result of the deflection of the crack path induced by the presence of the rigid CNC in the path of the growing crack. Since the CNC are well distributed, their presence affect all the sample. Thus, the surfaces of the composites are much rougher and no large agglomerates of CNC are observed in any of the images of the composites. This is also indicative that there is a good dispersion of the CNCs in the polymer, and good compatibility since no large aggregate unattached to the polymer can be observed (any potential small aggregates are well covered/attached to the polymer).

3.3.4. DSC characterization

DSC thermograms of the different samples were analyzed, and the data are summarized in Table 2, where ΔH (for both heatings and cooling) is given per weight of polymer in the sample as given by Eq. (11), where ΔH_{exp} is the value obtained from the experiment and ω the fraction of weight of polymer in the composite.

$$\Delta H = \frac{\Delta H_{exp}}{\omega} \tag{11}$$

The thermogram corresponding to the composite with 10 wt.% CNC is shown in Fig. 5(a) and is representative of all the thermograms obtained. The first heating shows multiple peaks during the fusion of the crystalline portion of the matrix, meaning that there are several types of crystals, with different melting temperatures, although the main melting event occurs at around 45 °C. In addition, it is remarkable that the same peaks can be found in the thermogram of the neat WBPU with approximately the same relation of sizes of the peaks, meaning that the addition of CNC affects all the different crystals in the same way. During the second heating, only one peak appears, with a small shoulder at lower temperature, and absence of a higher temperature peak. This last absence is probably due to a slower crystallization kinetics of those crystals that are not able to crystallize during the fast cooling. Most (but not all) of the crystallization occurs in the interval of crystallization

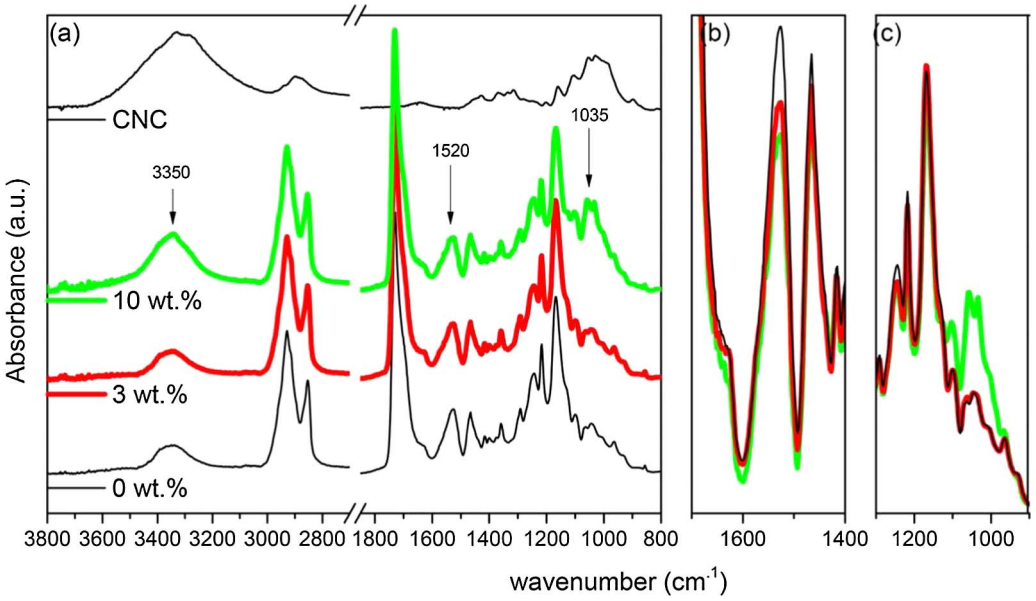

Fig. 3. FTIR of neat WBPU, pure CNC and the composites of CNC/WBPU (a) whole spectral range, (b and c) expanded scale of the regions where the main differences appear between neat PU and the composites.

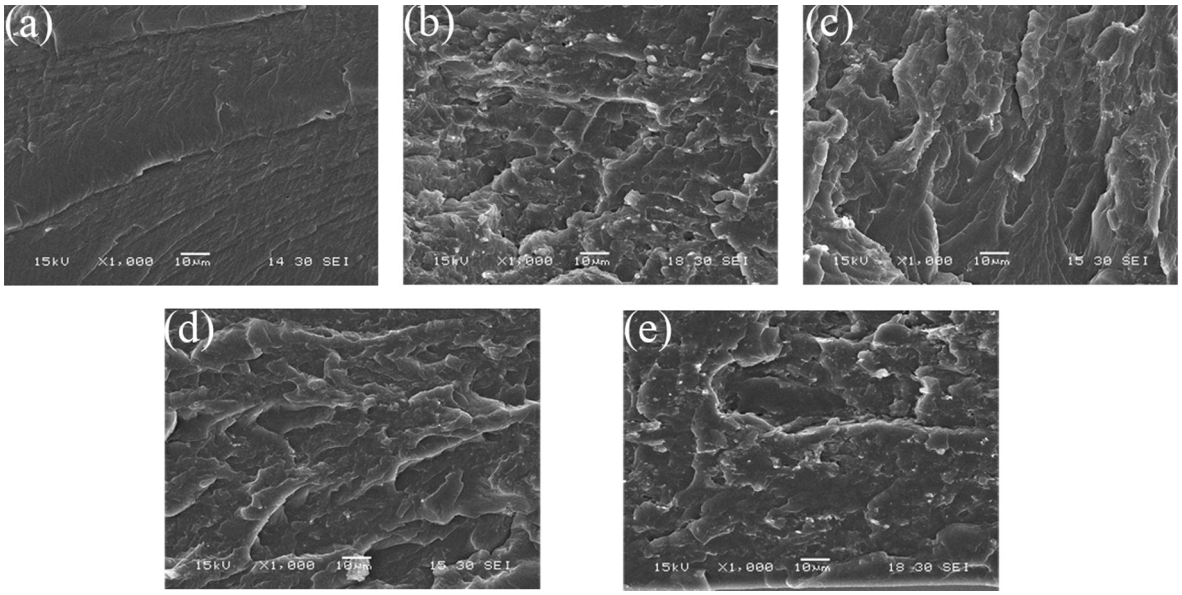

Fig. 4. SEM micrographs of fragile fracture surface of (a) neat WBPU, (b) 1 wt.%, (c) 3 wt.%, (d) 5 wt.% and (e) 10 wt.% of CNC.

observed during cooling. All the measured enthalpies (first and second heating and absolute value of the crystallization enthalpy) follow the same trend, with a decrease at 1 wt.% CNC, with respect to that of the neat polymer, followed by an increase to fall again a 10 wt.% CNC. It appears that the crystallization of the polymer is affected by the presence of the CNC, and the interference is particularly important when a high concentration is reached.

The changes in Tg due to the CNC observed during the first heating are not very large, but it seems that there is a correlation with the melting enthalpy. At 1 wt.%, the melting enthalpy decreases with respect to that of the neat PU and the Tg of the material also decreases. This observation indicates that the CNCs interfere with the crystallization of the polymer, resulting in higher mobility of the amorphous regions (lower glass transition). The presence of the nanocrystals in the matrix leads to the formation of polymer crystals that melt at higher temperature than those of the neat PU. This trend cannot be extended at the sample with 10 wt.% of CNC. In that sample, the Tm falls, probably because some aggregation of the CNCs, which reduces the interfacial interaction with the polymer.

When analyzing the cooling behavior, the reasoning is analogous. The data show a decrease in Tc as the concentration of CNC increases from 0 to 5 wt.% because of the lower mobility of the polymeric chains, requiring a higher subcooling to crystalize, except in the sample for the sample at 10 wt.% CNC, as already explained.

The trends described above are shown in the graphs in Fig. 5 where a clear similarity can be seen between both Tm and Tc (b), and ΔH and Tg (c). Similarly, the effects on Tg can be observed from the dynamic mechanical properties, as explained in the following section.

3.3.5. DMA

The storage modulus of the polyurethane and its nanocomposites decreases very slowly until the Tg of each sample is reached, then it shows a rapid decrease, which is the result of the mechanical relaxation related to the glass transition of the polymer as shown in Fig. 6 in the range of −50 °C to −40 °C [10,48]. The decrease observed after this relaxation is consistent with a material with incomplete phase separation (amorphous and crystalline phases), with the modulus showing a moderate and slow drop because of the presence of the crystals. In this region, the effect of the CNC can be seen, and as expected, the relative modulus increases with the concentration of CNC in the nanocomposite film. Around 40 °C, the storage modulus of the pure WBPU shows a more important drop, which is consistent with its lineal structure and the melting of the polyurethane soft segments that were acting as crosslinking points up to Tm (in agreement with the thermal behavior observed by DSC). All the nanocomposites show this rather drastic drop of the modulus at the Tm of the polymer. Additionally, the storage modulus of the samples containing higher contents of the CNC becomes almost a plateau, even above the melting temperature, which indicates that a percolated network of CNC has been formed and that its strength is high enough to sustain the material in the range of temperatures analyzed.

The effect of the CNC on the dynamic mechanical response of the materials extends through all the temperature range analyzed. Thus, at −90 °C the E′ of the nanocomposite with 10 wt.% of CNC is more than 140% the value corresponding to the pure WBPU (3260 and 2180 MPa respectively), and this difference grows to about 640% at 35 °C (316 and 48 MPa respectively).

Table 2
DSC data of neat WBPU and the composites.*

CNC content (wt.%)	1st Heating			Cooling		2nd Heating		
	Tg (°C)	Tm (°C)	ΔH (kJ g_{PU}^{-1})	Tc (°C)	ΔH (kJ g_{PU}^{-1})	Tg (°C)	Tm (°C)	ΔH (kJ g_{PU}^{-1})
0	−45.2	45.5	43.5	7.2	−32.1	–	41.5	42.1
1	−46.2	46.8	41.7	7.1	−31.1	−42.7	42.9	38.5
3	−45.0	48.2	43.1	6.9	−32.2	−46.0	43.6	38.7
5	−44.5	49.7	44.2	6.6	−32.2	−41.6	46.1	40.8
10	−44.5	45.1	42.8	8.2	−29.7	−45.4	42.2	36.1

* The heat of melting and crystallization is given per weight of the polymer in the sample.

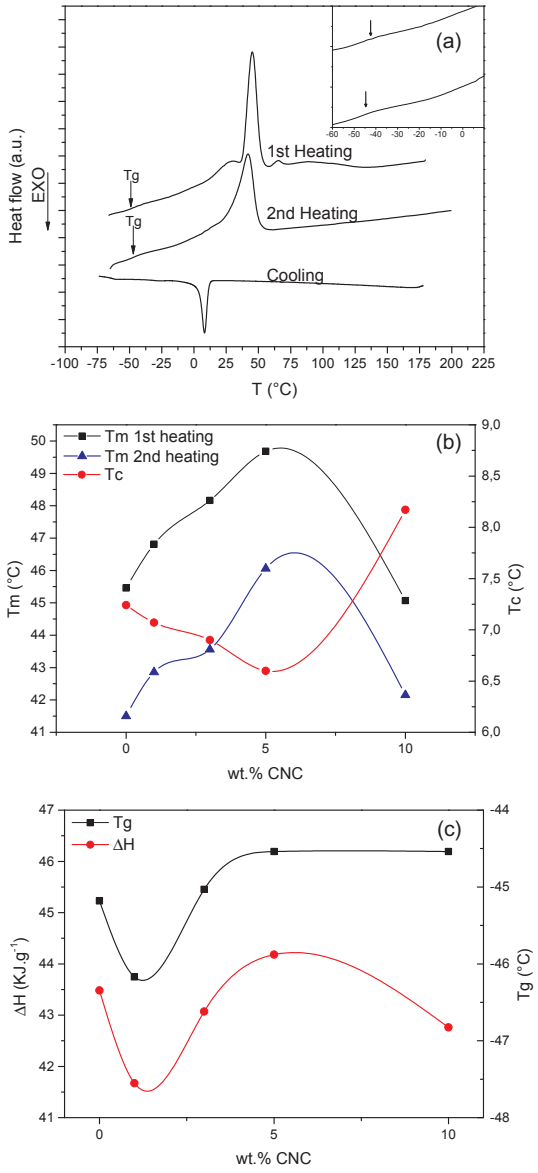

Fig. 5. (a) Thermogram of the composite with 10 wt.% CNC, showing the representative thermal behavior of all the composites and data from DSC curves showing similar trends, (b) Tm and Tc and (c) Tg and ΔH.

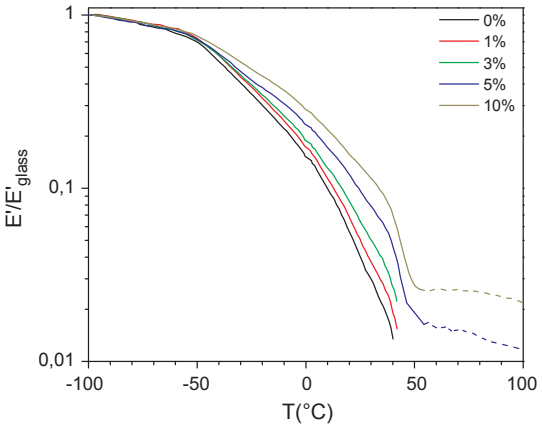

Fig. 6. Relative storage modulus (E′/ E′ glass) versus temperature, with E′ glass measured at −100 °C for neat WBPU and composites.

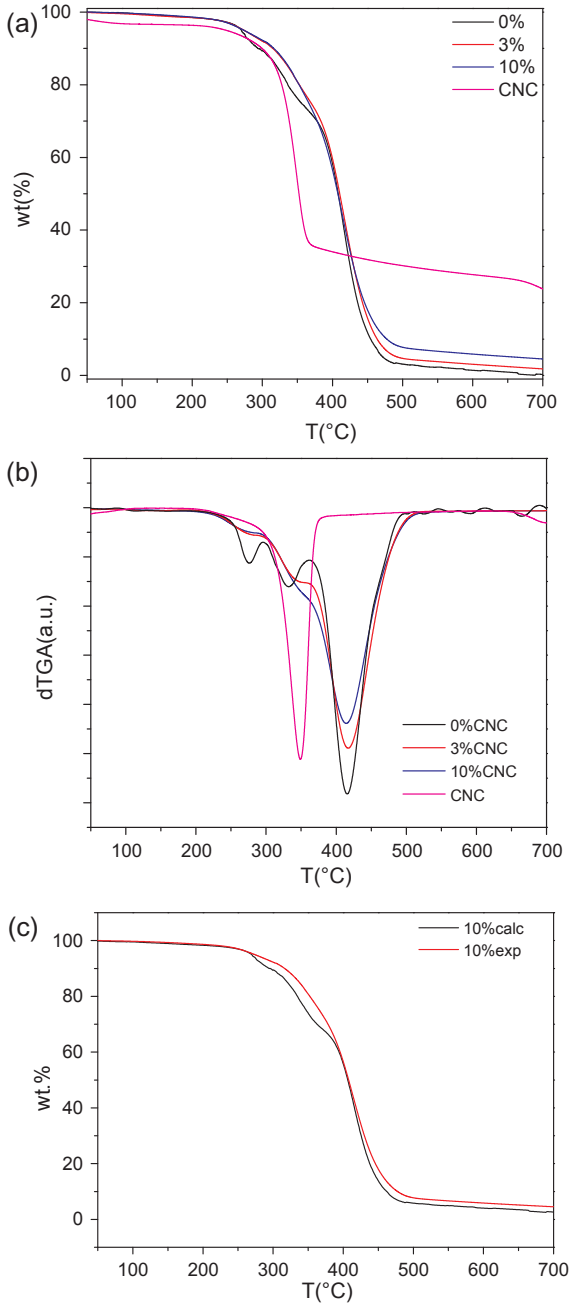

Fig. 7. (a) TGA and (b) derivative signal of selected samples. (c) Calculated and experimental TGA curves of the composite with 10 wt.% of CNC.

3.3.6. TGA

Fig. 7 illustrates the thermal degradation behavior of the samples. The thermogram (and derivative signal) of the pure WBPU show a first loss around 275 °C and a second at 330 °C, which becomes a small shoulder slightly shifted to higher temperatures in the curves of the composites. The mass loss of the neat CNC occurs between 200 and 300 °C, which is lower than that of pure cellulose, because of the effects of the sulfuric acidolysis on the processes of depolymerization, dehydration and decomposition of glycosyl units. This is also the reason for the comparatively high char (presence of sulfate groups in the surface of the CNC). In the TGA (and dTGA) curves corresponding to the composites, there are no additional steps compared to those observed for the neat polymer [48]. The main degradation peak appears at 415 °C in all samples and this temperature is not much affected by the presence of CNC in the polymeric material. The decomposition of the unfilled

Table 3
TGA data of the neat WBPU and composites.

CNC (wt.%)	$T_{5\%}$	$T_{10\%}$	Char (%)
0	270	293.75	0.02
3	274	314	0.78
10	273	316	3.44

polyurethane shows the typical decomposition steps: the first loss (240–300 °C) can be assigned to the breaking of urethane bonds, while the second (300–370 °C) is related to the decomposition of the segments from the polyol, and the third (370–500 °C), to the cleavage of C-C bonds and other segments of the structure [49–52]. In the case of the composites, the first and second decomposition steps of the polyurethanes are largely subdued and the main decomposition remains centered at 415 °C as mentioned before. Finally, the remaining char measured at 800 °C for the pure WBPU is 0.05%, while it is 0.78% for the composite with 3 wt.% CNC and 3.4% for the 10 wt.% nanocomposite. The higher thermal stability of the nanocomposites (higher onset of degradation and higher char than the neat WBPU as more CNC is incorporated, Table 3) together with the absence of a separate peak that could be assigned to cellulose degradation are indicative of a good interaction between the filler and the matrix. To confirm this last statement, a TG curve of the composite with 10 wt.% of CNC was calculated (predicted) from the weighed traces experimentally obtained for the neat compounds, cellulose nanocrystals and WBPU, using Eq. (12)

$$TG(composite 10\ \text{wt. \%}\ CNC) = 0.9 \times TG(WBPU) + 0.1 \times TG(CNC) \quad (12)$$

As shown in Fig. 7c, the calculated TG curve is different quantitatively, but also qualitatively from the experimental result, since essentially a single main step degradation appears in the experimental curve while the three steps corresponding to the polyurethane degradation are visible in the calculated curve. This means that there is, in fact, an interaction between the WBPU and the CNC. It can also be interpreted as a positive interaction since the experimental onset of degradation is shifted towards higher temperature with respect to the calculated TG curve.

3.3.7. Mechanical properties

The strain-stress curves obtained from tensile tests (Fig. 8(a)) show an initial elastic region at small deformations and a large region of plastic deformation until failure. In particular, the samples with low content of CNC (0, 1 and 3 wt.%) show a clear yield point, while the others (5 and 10 wt.%) do not. CNCs show a high efficiency as reinforcing filler in these nanocomposites. The results are shown in Fig. 8(b) and (c). The reported values of the tensile modulus of the composites show an important dependence with the amount of CNC added, increasing almost 900% from the pure WBPU to the composite with 10 wt.% CNC. This observation is in clear agreement with the increase of the storage modulus at room temperature as it was already discussed. However, the presence of CNCs in the composite has a negative effect in the extensibility of the material, but even for the sample with the highest CNC concentration (10 wt.%), the strain at break is higher than 150%, and in the one with 5 wt.%, it raises to over 500%; thus, all the materials are highly extensible. The tensile strength is almost constant when the CNC content is lower than 5 wt.%, showing then an important increase of around 40%. It has been reported [53–55] that the efficiency of the filler depends on the capacity to form a percolated network and in this case, it seems that this condition is achieved between 3 wt.% and 5 wt.%, because of the raise in the stress at break and the change in the trend of the modulus, also evidenced in the already analyzed DMA essays, and also in the thermal behavior of the composite films (DSC), in which agglomeration was proposed at higher concentrations (10 wt.% of CNC).

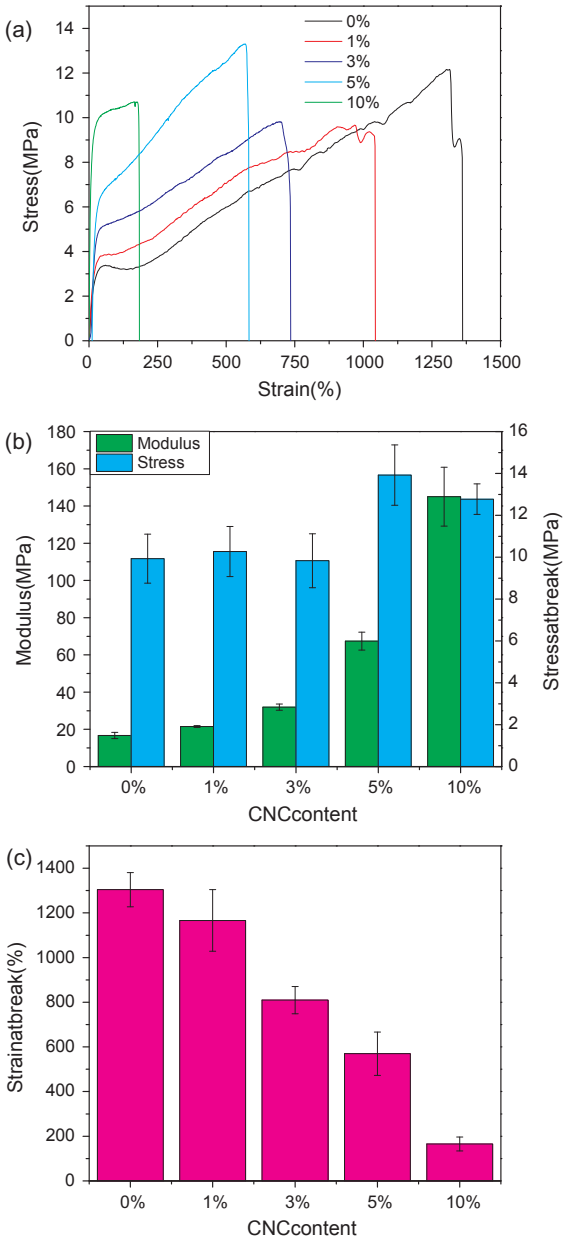

Fig. 8. (a) Representative strain v stress curves of the neat WBPU and composites and (b and c) results from the tensile tests.

3.3.8. Mechanical properties modelling

For a better understanding of the interaction between WBPU and CNCs, and the presence of a percolation threshold, the modulus and stress at yield experimental data were fitted using two models, as shown in Fig. 9. Regarding modulus data, both Hirsch and Ouali models can represent the behavior of the composites with reasonably accuracy. As already explained, the Ouali model defines φ_v as the critical concentration at which the percolation is reached and shows a clear change in the function that is coherent with the experimental results obtained. The theoretical percolation threshold calculated using Eq. (9) and the average aspect ratio measured in this work is 1.3 vol.% (~1.8 wt.%), which is below the experimental value, ~2 vol.% (~3 wt.%). This result is in good agreement with other literature reports that show that the experimental value appears above the theoretical one because of the presence of agglomerates [3]. For the calculations, the modulus of the matrix was taken from the experimental data for the sample with 0 vol.

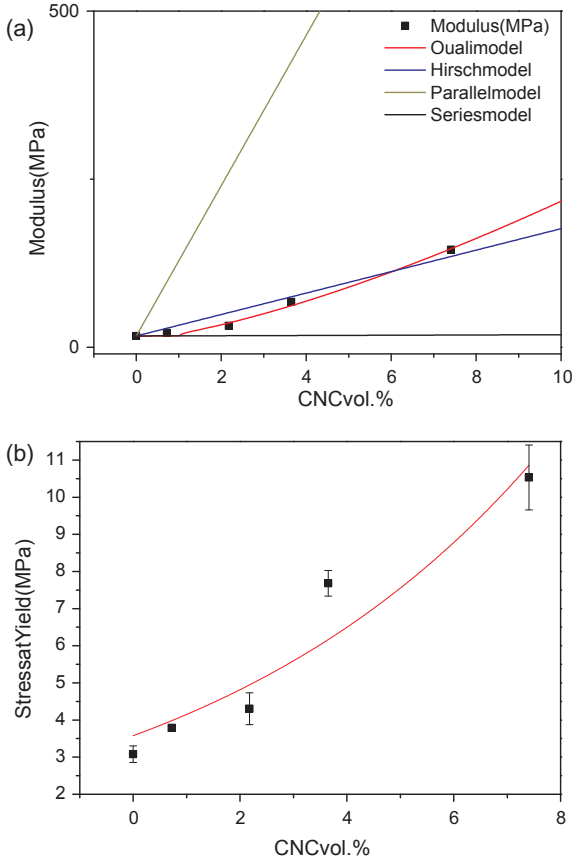

Fig. 9. Modelling of (a) the modulus data and (b) stress at yield of the composites using Pukanszky model.

% CNC, meaning neat WBPU, and equal to 16.68 MPa, while the modulus of the percolating network of CNC was left as fitting parameter of the models. The best fitting value was 11.2 GPa for Hirsch model, which is within the intervals reported in other studies, and the parameter x is 0.14. However, the CNC modulus fitted according to the Ouali model was 5.7 GPa, which is rather low for a cellulose network [56,57]. On the other hand the last model gives a slightly better fit of the data.

For the strength of the composites, the stress at yield was fitted using Pukanszky model as already explained. The curve shown was fitted using a value of B of 18.32, which is a value much higher than 3, indicating that the interface is strong and the reinforcing effect is noteworthy [37].

4. Conclusions

In this work, a macrodiol derived from castor oil was used to synthesize a WBPU, with a high content of bio-based carbon. On the other hand, CNCs were obtained by acid hydrolysis from cellulose nanofibers. The rod-like CNCs with aspect ratio of 52.9 ± 19.4 were used as fillers in the composites. The films obtained by casting were in all cases transparent (even the one with 10 wt.% of CNCs) and had better mechanical and thermal properties than the neat WBPU, increasing the storage modulus (between 1.4 and 6.4 times depending on temperature, for the composite with 10 wt% CNC), elastic modulus (almost 9 times the value of the WBPU) and strength (about 40% higher in the 5 wt.% of CNC sample). The degradation properties were improved as well. Finally, the mechanical properties were fitted using simple models, showing a percolation threshold, around 2 vol.% (~3 wt.%), the same value estimated from dynamic-mechanical data. Additionally, good compatibility between PU and CNC was also supported by the analysis of SEM micrographs that showed well dispersed systems and absence of non-attached aggregates of CNC.

Acknowledgments

The authors acknowledge the funding from CONICET (PIP 0866), ANPCyT (PICT 140732) and UNMdP (15/G430-ING436/15). J.M. Buffa thanks CONICET for a fellowship grant. Also, the People Programme (Marie Curie Actions-International Research Staff Exchange Scheme) of the European Union's Seventh Framework Programme under REA grant agreement number PIRSES-GA-2012-318996, titled "Bio-based polyurethane composites with natural fillers" (Acronym: BIOPURFIL). Moreover, the authors thank the University of the Basque Country UPV/EHU for the technical and human support provided by SGIker Macro behaviour-Mesostructure-Nanotechnology and Basque Country Government in the frame of Consolidated Groups (IT-776-13) and the Spanish Ministry of Economy and Competitiveness (MINECO) (MAT2016-76294-R).

References

[1] O.J. Rojas, O.J.R. Editor, Cellulose Chemistry and Properties: Fibers, Nanocelluloses and Advanced Materials, 1st ed., Springer, 2016.
[2] T. Abitbol, A. Rivkin, Y. Cao, Y. Nevo, E. Abraham, T. Ben-Shalom, S. Lapidot, O. Shoseyov, Nanocellulose, a tiny fiber with huge applications, Curr. Opin. Biotechnol. 39 (2016) 76–88, http://dx.doi.org/10.1016/j.copbio.2016.01.002.
[3] X. Xu, F. Liu, L. Jiang, J.Y. Zhu, D. Haagenson, D.P. Wiesenborn, Cellulose nanocrystals vs. cellulose nanofibrils: a comparative study on their microstructures and effects as polymer reinforcing agents, ACS Appl. Mater. Interfaces 5 (2013) 2999–3009, http://dx.doi.org/10.1021/am302624t.
[4] S.J. Eichhorn, A. Dufresne, M.I. Aranguren, N.E. Marcovich, J.R. Capadona, S.J. Rowan, C. Weder, W. Thielemans, M. Roman, S. Renneckar, W. Gindl, S. Veigel, J. Keckes, H. Yano, K. Abe, M. Nogi, a. N. Nakagaito, A. Mangalam, J. Simonsen, a. S. Benight, A. Bismarck, L. a. Berglund, T. Peijs, Review: current international research into cellulose nanofibres and nanocomposites, 2010. doi: 10.1007/s10853-009-3874-0.
[5] O. Nechyporchuk, M. Naceur, J. Bras, Production of cellulose nanofibrils: a review of recent advances, Ind. Crop. Prod. (2016), http://dx.doi.org/10.1016/j.indcrop.2016.02.016.
[6] K.C. Yong, Y.C. Ching, A. Mohamad, Z.K. Lim, K.E. Chong, Mechanical and thermal properties of chemical treated oil palm empty fruit bunches fiber reinforced polyvinyl alcohol composite, J. Biobased Mater. Bioenergy 9 (2015) 231–235.
[7] S. Olivera, H.B. Muralidhara, K. Venkatesh, V.K. Guna, K. Gopalakrishna, Y. Kumar, Potential applications of cellulose and chitosan nanoparticles/composites in wastewater treatment: a review, Carbohydr. Polym. 153 (2016) 600–618, http://dx.doi.org/10.1016/j.carbpol.2016.08.017.
[8] J. George, Cellulose nanocrystals: synthesis, functional properties, and applications, Nanotechnol. Sci. Appl. 8 (2015) 45–54.
[9] N. Lavoine, I. Desloges, A. Dufresne, J. Bras, Microfibrillated cellulose – its barrier properties and applications in cellulosic materials: a review, Carbohydr. Polym. 90 (2012) 735–764, http://dx.doi.org/10.1016/j.carbpol.2012.05.026.
[10] Y.C. Ching, M. Ershad Ali, L.C. Abdullah, K.W. Choo, Y.C. Kuan, S.J. Julaihi, C.H. Chuah, N.-S. Liou, Rheological properties of cellulose nanocrystal-embedded polymer composites: a review, Cellulose (2016), http://dx.doi.org/10.1007/s10570-016-0868-3.
[11] S. Iwamoto, W. Kai, A. Isogai, T. Iwata, Elastic modulus of single cellulose microfibrils from tunicate measured by atomic force, Microscopy (2009) 2571–2576.
[12] X. Wu, R.J. Moon, A. Martini, Tensile strength of I b crystalline cellulose predicted by molecular dynamics simulation (2014) 2233–2245, http://dx.doi.org/10.1007/s10570-014-0325-0.
[13] T. Nishino, K. Takano, K. Nakamae, Elastic modulus of the crystalline regions of cellulose polymorphs, J. Polym. Sci. Part B Polym. Phys. 33 (1995) 1647–1651.
[14] F. Tanaka, T. Iwata, Estimation of the elastic modulus of cellulose crystal by molecular mechanics simulation, 2006, 509–517. doi: 10.1007/s10570-006-9068-x.
[15] A. Pakzad, J. Simonsen, R.S. Yassar, Gradient of nanomechanical properties in the interphase of cellulose nanocrystal composites, Compos. Sci. Technol. 72 (2012) 314–319, http://dx.doi.org/10.1016/j.compscitech.2011.11.020.
[16] N. Yildrim, S. Shaler, The application of nanoindentation for determination of cellulose nano fi brils (CNF) nanomechanical properties, Mater. Res. Express. 3 (2016) 1–10, http://dx.doi.org/10.1088/2053-1591/3/10/105017.
[17] A. Dufresne, Nanocellulose: a new ageless bionanomaterial, Mater. Today 16 (2013) 220–227, http://dx.doi.org/10.1016/j.mattod.2013.06.004.
[18] M. Mariano, N. El Kissi, A. Dufresne, Cellulose nanocrystals and related nanocomposites: review of some properties and challenges, J. Polym. Sci. Part B Polym. Phys. 52 (2014) 791–806, http://dx.doi.org/10.1002/polb.23490.
[19] M.O. Seydibeyoglu, K. Oksman, Novel nanocomposites based on polyurethane and micro fibrillated cellulose, Compos. Sci. Technol. 68 (2008) 908–914, http://dx.doi.org/10.1016/j.compscitech.2007.08.008.
[20] X. Zhang, R. Xu, Z. Wu, C. Zhou, The synthesis and characterization of

polyurethane/clay nanocomposites, Polym. Int. 52 (2003) 790–794.
[21] M.E.V. Hormaiztegui, V.L. Mucci, A. Santamaria-Echart, M.A. Corcuera, A. Eceiza, M.I. Aranguren, Waterborne polyurethane nanocomposites based on vegetable oil and microfibrillated cellulose, J. Appl. Polym. Sci. 44207 (2016) 1–12, http://dx.doi.org/10.1002/app.44207.
[22] A. Santamaria-Echart, L. Ugarte, A. Arbelaiz, N. Gabilondo, M.A. Corcuera, A. Eceiza, Two different incorporation routes of cellulose nanocrystals in waterborne polyurethane nanocomposites, Eur. Polym. J. 76 (2016) 99–109, http://dx.doi.org/10.1016/j.eurpolymj.2016.01.035.
[23] X. Cao, C. Xu, Y. Wang, Y. Liu, Y. Liu, Y. Chen, New nanocomposite materials reinforced with flax cellulose nanocrystals in waterborne polyurethane, Biomacromolecules 8 (2007) 889–904, http://dx.doi.org/10.1016/j.polymertesting.2013.04.005.
[24] Y. Li, A.J. Ragauskas, Cellulose nano whiskers as a reinforcing filler in polyurethanes, Adv. Divers. Ind. Appl. Nanocomposites (2011) 17–36.
[25] V. Kumar, R. Bollström, A. Yang, Q. Chen, G. Chen, P. Salminen, D. Bousfield, M. Toivakka, Comparison of nano- and microfibrillated cellulose films, Cellulose 21 (2014) 3443–3456, http://dx.doi.org/10.1007/s10570-014-0357-5.
[26] A. Saralegi, L. Rueda, B. Fernández d'Arlas, I. Mondragon, A. Eceiza, M.A. Corcuera, Thermoplastic polyurethanes from renewable resources: effect of soft segment chemical structure and molecular weight on morphology and final properties, Polym. Int. 62 (2013) 106–115, http://dx.doi.org/10.1002/pi.4330.
[27] G. Mondragon, C. Peña-Rodriguez, A. González, A. Eceiza, A. Arbelaiz, Bionanocomposites based on gelatin matrix and nanocellulose, Eur. Polym. J. 62 (2015) 1–9, http://dx.doi.org/10.1016/j.eurpolymj.2014.11.003.
[28] J.M. Buffa, M.A. Grela, M.I. Aranguren, V. Mucci, EPR spectroscopy applied to the study of the TEMPO mediated oxidation of nanocellulose, Carbohydr. Polym. 136 (2016) 744–749, http://dx.doi.org/10.1016/j.carbpol.2015.09.094.
[29] S.A. Madbouly, Y. Xia, M.R. Kessler, Rheological behavior of environmentally friendly castor oil-based waterborne polyurethane dispersions, Macromolecules 46 (2013) 4606–4616.
[30] A. Saralegi, M.L. Gonzalez, A. Valea, A. Eceiza, M.A. Corcuera, The role of cellulose nanocrystals in the improvement of the shape-memory properties of castor oil-based segmented thermoplastic polyurethanes, Compos. Sci. Technol. 92 (2014) 27–33, http://dx.doi.org/10.1016/j.compscitech.2013.12.001.
[31] A.D. French, Idealized powder diffraction patterns for cellulose polymorphs, Cellulose 21 (2014) 885–896, http://dx.doi.org/10.1007/s10570-013-0030-4.
[32] S. Park, J.O. Baker, M.E. Himmel, P.A. Parilla, D.K. Johnson, Cellulose crystallinity index: measurement techniques and their impact on interpreting cellulase performance, Biotechnol. Biofuels 3 (2010) 10, http://dx.doi.org/10.1186/1754-6834-3-10.
[33] Y.M. Zhou, S.Y. Fu, L.M. Zheng, H.Y. Zhan, Effect of nanocellulose isolation techniques on the formation of reinforced poly(vinyl alcohol) nanocomposite films, Express Polym. Lett. 6 (2012) 794–804, http://dx.doi.org/10.3144/expresspolymlett.2012.85.
[34] N.E. Marcovich, M.M. Reboredo, M.I. Aranguren, Modified woodflour as thermoset fillers ii. Thermal degradation of woodflours and composites, Thermochim. Acta 372 (2001) 45–57, http://dx.doi.org/10.1016/S0040-6031(01)00425-7.
[35] M. Pereda, A. Dufresne, M.I. Aranguren, N.E. Marcovich, Polyelectrolyte films based on chitosan/olive oil and reinforced with cellulose nanocrystals, Carbohydr. Polym. 101 (2014) 1018–1026.
[36] J. Xiong, R. Mashiur, Mechanical property measurement and prediction using Hirsch's model for glass yarn reinforced polyethylene composite fabric formwork, J. Text. Sci. Eng. 6 (2016) 1–9, http://dx.doi.org/10.4172/2165-8064.1000241.
[37] U. Casado, N.E. Marcovich, M.I. Aranguren, M.A. Mosiewicki, High-Strength Composites Based on Tung Oil Polyurethane and Wood Flour : Effect of the Filler Concentration on the Mechanical Properties, 2009, doi: 10.1002/pen.
[38] B. Pukanszky, F. Tudos, J. Jancar, J. Kolarik, The possible mechanisms of polymer-filler interaction in polypropylene-$CaCO_3$ composites, J. Mater. Sci. Lett. 8 (1989) 1040–1042.
[39] Y. Zare, Composites: Part B New models for yield strength of polymer/clay nanocomposites, Composites Part B 73 (2015) 111–117, http://dx.doi.org/10.1016/j.compositesb.2014.12.026.
[40] D. Metin, F. Tihminlioglu, D. Balkose, S. Ulku, The effect of interfacial interactions on the mechanical properties of polypropylene/natural zeolite composites, Composites Part A Appl. Sci. Manuf. 35 (2004) 23–32, http://dx.doi.org/10.1016/j.compositesa.2003.09.021.
[41] D.A. Prokhorova, A.P. Chatterjee, Elastic Moduli of Cellulose Nanoparticle-Reinforced Composites : A Micromechanical Model, 2009, pp. 3259–3265.
[42] C. Bilbao-Sainz, J. Bras, T. Williams, T. Senechal, W. Orts, HPMC reinforced with different cellulose nano-particles, Carbohydr. Polym. 86 (2011) 1549–1557, http://dx.doi.org/10.1016/j.carbpol.2011.06.060.
[43] C. Schütz, M. Agthe, A.B. Fall, K. Gordeyeva, V. Guccini, M. Salajková, T.S. Plivelic, J.P.F. Lagerwall, G. Salazar-Alvarez, L. Bergström, Rod packing in chiral nematic cellulose nanocrystal dispersions studied by small-angle X-ray scattering and laser diffraction, Langmuir 31 (2015) 6507–6513, http://dx.doi.org/10.1021/acs.langmuir.5b00924.
[44] M.A. Hubbe, O.J. Rojas, L.A. Lucia, M. Sain, Cellulosic nanocomposites: a review, BioResources 3 (2008) 929–980, http://dx.doi.org/10.15376/biores.3.3.929-980.
[45] D.M. do Nascimento, J.S. Almeida, M. do, S. Vale, R.C. Leitão, C.R. Muniz, M.C.B. de Figueirêdo, J.P.S. Morais, M.D.F. Rosa, D.M.J.S. Almeida, S. Vale, R.C. Leitão, C.R. Muniz, M. Clea, B. De Figueirêdo, J. Paulo, S. Morais, M.D.F. Rosa, A comprehensive approach for obtaining cellulose nanocrystal from coconut fiber. Part I: Proposition of technological pathways, Ind. Crop. Prod. (2016), http://dx.doi.org/10.1016/j.indcrop.2015.12.078.
[46] G. Socrates, Infrared and Raman characteristic group frequencies, 2004. doi: 10.1002/jrs.1238.
[47] H. Du, Y. Zhao, Q. Li, J. Wang, M. Kang, X. Wang, H. Xiang, Synthesis and characterization of waterborne polyurethane adhesive from MDI and HDI, J. Appl. Polym. Sci. 110 (2008) 1396–1402, http://dx.doi.org/10.1002/app.
[48] X. Cao, Y. Habibi, L.A. Lucia, One-pot polymerization, surface grafting, and processing of waterborne polyurethane-cellulose nanocrystal nanocomposites, J. Mater. Chem. 19 (2009) 7137–7145, http://dx.doi.org/10.1039/b910517d.
[49] E. Głowińska, J. Datta, Bio polyetherurethane composites with high content of natural ingredients: hydroxylated soybean oil based polyol, bio glycol and microcrystalline cellulose, Cellulose (2015), http://dx.doi.org/10.1007/s10570-015-0825-6.
[50] M. Lee, M. Haeng, H. Lee, Y. Kim, J. Shin, Tunable softening and toughening of individualized cellulose nanofibers-polyurethane urea elastomer composites, Carbohydr. Polym. 159 (2017) 125–135, http://dx.doi.org/10.1016/j.carbpol.2016.12.019.
[51] M.A. Corcuera, L. Rueda, B. Fernandez d́Arlas, A. Arbelaiz, C. Marieta, I. Mondragon, A. Eceiza, Microstructure and properties of polyurethanes derived from castor oil, Polym. Degrad. Stab. 95 (2010) 2175–2184, http://dx.doi.org/10.1016/j.polymdegradstab.2010.03.001.
[52] I. Ganetri, A. Oulmidi, N. Dardouri, A. Challioui, L. Tighzert, P. Dony, Biocomposites based on castor oil polyurethane and organosilane modified cellulose fibers, J. Mater. Environ. Sci. 7 (2016) 3740–3749.
[53] G.H.D. Tonoli, E.M. Teixeira, A.C. Correa, J.M. Marconcini, L.A. Caixeta, M.A. Pereira-Da-Silva, L.H.C. Mattoso, Cellulose micro/nanofibres from Eucalyptus kraft pulp: preparation and properties, Carbohydr. Polym. 89 (2012) 80–88, http://dx.doi.org/10.1016/j.carbpol.2012.02.052.
[54] P.S. De Oliveira Patricio, I.M. Pereira, N.C.F. Da Silva, E. Ayres, F.V. Pereira, R.L. Oréfice, Tailoring the morphology and properties of waterborne polyurethanes by the procedure of cellulose nanocrystal incorporation, Eur. Polym. J. 49 (2013) 3761–3769, http://dx.doi.org/10.1016/j.eurpolymj.2013.08.006.
[55] T. Pullawan, A.N. Wilkinson, S.J. Eichhorn, Discrimination of matrix-fibre interactions in all-cellulose nanocomposites, Compos. Sci. Technol. 70 (2010) 2325–2330, http://dx.doi.org/10.1016/j.compscitech.2010.09.013.
[56] K. Das, D. Ray, N.R. Bandyopadhyay, T. Ghosh, A.K. Mohanty, M. Misra, A study of the mechanical, thermal and morphological properties of microcrystalline cellulose particles prepared from cotton slivers using different acid concentrations, Cellulose 16 (2009) 783–793, http://dx.doi.org/10.1007/s10570-009-9280-6.
[57] M. Henriksson, L.A. Berglund, P. Isaksson, T. Lindstrom, T. Nishino, Cellulose nanopaper structures of high toughness, Biomacromolecules 9 (2008) 1579–1585.